

# Electromagnetic Design of Propulsion Motors with Superconducting Field Coils for Electrified Aircraft



Yusuke Ishida, Yutaka Terao, and Hiroyuki Ohsaki

## 1 Introduction

In recent years the demand for passenger and cargo transportation aircraft has been increasing, and the reduction of carbon dioxide emissions from aircraft is required. In such a situation, aircraft electrification is currently studied worldwide [1–3]. And the electrification of propulsion system, called electrified aircraft propulsion system (EAPS), has attracted much attention. The EAPS uses electric motors to drive fans and has potential to achieve higher efficiency and less greenhouse gas emissions than conventional internal combustion propulsion systems. However, in order to realize the EAPS, electric motors are required to achieve a high output density. Since electric vehicles, such as cars and motor bikes, have become popular, the high-performance permanent magnet-type synchronous motors have been developed as compact, lightweight, and efficient machines. The permanent magnet-type synchronous motor having the world's highest output power density of 5.2 kW/kg is the model, SP260D manufactured for 260 kW applications by Siemens [3]. However, the output power density of motors to be loaded into EAPS must surpass 16 kW/kg for aircraft with more than 100 passengers [4]. Therefore, there are many technical issues for conventional motors to achieve such a high output power density. Thus, adopting superconducting motors for EAPS is considered in this study to reach the specified value for output power density.

The property of superconducting materials to have zero resistance below a critical temperature provides superconducting wires to have much higher current density than it would be possible in copper windings. The typical wound-rotor synchronous motors are composed of copper windings and iron cores. Adapting

---

Y. Ishida (✉) · Y. Terao · H. Ohsaki  
The University of Tokyo, Tokyo, Japan  
e-mail: [ishida-yusuke537@g.ecc.u-tokyo.ac.jp](mailto:ishida-yusuke537@g.ecc.u-tokyo.ac.jp); [yterao8934@g.ecc.u-tokyo.ac.jp](mailto:yterao8934@g.ecc.u-tokyo.ac.jp);  
[ohsaki@k.u-tokyo.ac.jp](mailto:ohsaki@k.u-tokyo.ac.jp)

superconducting wires to wound-rotor synchronous motors enables motors to reduce not only the amount of windings but also the amount of irons because the superconducting coils are able to achieve higher air-gap magnetic flux density without the need of iron cores of rotor and without iron teeth. Thus, high output power density synchronous motors can be realized [5].

In this study, we conducted the electromagnetic design of propulsion motors with superconducting field coils and copper armature windings, partially superconducting motor (PSCM), to be used in EAPS based on analytical equations. PSCMs have small electric loadings and relatively become heavier than fully superconducting motors (FSCMs), which have superconducting field coils and armature windings. The FSCMs have AC loss, which is proportional to frequency. Therefore, the FSCMs should be designed with a smaller number of poles. However, the PSCMs have the possibility of achieving high output density and efficiency simultaneously by increasing number of poles because the PSCMs have no AC loss at armature windings unlike the FSCMs.

The objective of this work is to verify whether PSCMs are able to attain high output density. We optimized only the output density of the PSCMs in the design dominantly. After optimization, the finite element method (FEM) analysis is carried out for the purpose of testifying that the analytical design achieves calculated output density.

## 2 Electrified Aircraft Propulsion System Configuration

Figure 1 shows an EAPS configuration. The hybrid AC-DC architecture is employed [6]. The whole system is composed of two turbines and generators on both wings, converters, DC bus, inverters, and several distributed PSCMs. The electric power is

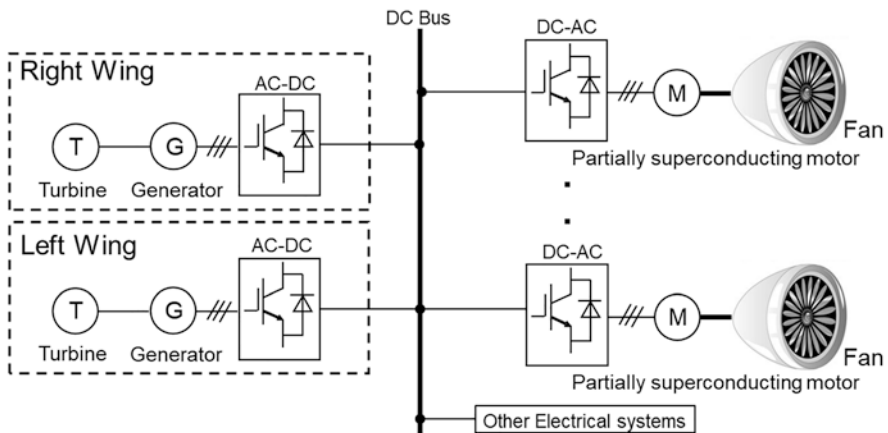


**Fig. 1** Electrified aircraft propulsion system configuration

generated by the turbine and generator. The DC bus provides DC power to electrical systems in the aircraft and to the superconducting motor drive systems via converters. In order to drive the superconducting motors, DC power is converted to three-phase AC power via the inverter. The EAPS is supposed to adopt superconducting technologies. Using a superconducting DC bus power supply reduces AC loss in the cables. This improves to the efficiency of the aircraft. Several distributed superconducting motors mounted on the propulsion system provide high redundancy for the aircraft.

### 3 Partially Superconducting Motor Specifications

The PSCM's basic specifications we considered are summarized in Table 1. We considered that the total output power for 180-passenger class aircraft as 44 MW for takeoff [7] and all the output powers are provided from several PSCMs. Therefore, the output power of 5.5 MW means that eight motors are required to satisfy the total output power for aircraft. The line-to-line voltage is set at 1.41 kV, and this is relatively higher than that of today's aircraft considering the problem of electric breakdown in thin atmospheric pressure conditions [8]; however, there are some attempts to increase the voltage of aircraft's electric systems [6]. The rotational speed is set at 5000 rpm and this value is based on the low pressure turbine of conventional turbo-fan engines.

Figure 2 shows the basic configuration of a PSCM. The PSCM is composed of very low temperature YBCO superconducting field coils and room temperature copper armature windings. The superconducting field coils are covered with cryostat for thermal insulating. The cryostat and field coils are connected through a thin cylinder called torque tube. The torque tube should have high mechanical strength to transfer high torque from field coils to the shaft and low thermal conductivity to suppress the heat leakage into the low temperature part. The rotor rotates synchronously with the rotating field produced by armature currents in the stator, and the magnetic flux density at the field coils is not changed over time under steady-state condition except the AC field harmonics. Therefore, the YBCO wire is suitable for

**Table 1** Specifications for PSCM

Description	Value
Motor output power	5.5 MW
Line-to-line voltage	1.41 kV
Torque	10,504 nm
Rotational speed	5000 rpm
Number of poles	8–14
Magnetic loading	0.4–1.2 T
Electric loading	120 kA/m
Motor diameter	<800 mm

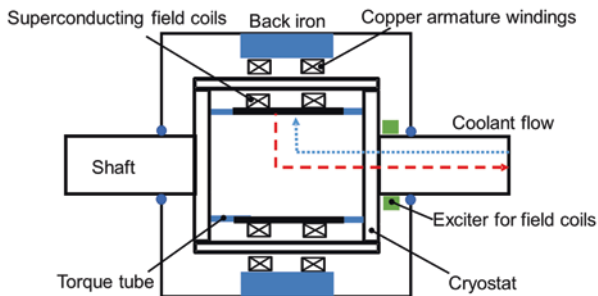


Fig. 2 Configuration of a partially superconducting motor

Table 2 Details for field coils and armature windings

Parameter	Value
Field coils	YBCO
Operating temperature	20, 65 K
Configuration	4.0 mm × 0.1 mm rectangle
Packing factor	0.95
Load factor	0.7
Armature windings	Copper
Operating temperature	300 K
Configuration	2.5 mm × 0.4 mm rectangle
Conductor current density	$2.5 \times 10^7$ A/m <sup>2</sup>
Packing factor	0.4

the field coils that have good  $J_c$ - $B$  characteristics, mechanical strength, and large temperature margins. The details of the field coils and the armature windings are summarized in Table 2. The critical current of the YBCO wires used in this study is based on the wire from SuperPower Inc. [9]. Assumed critical current densities of the YBCO wire at different magnetic flux densities are shown in Fig. 3. The copper wire used in this study is considered to enhance its current density due to the water cooling.

As mentioned previously, the superconducting motor achieves high air-gap magnetic flux density, and the iron teeth do not serve a significant role in the motor. Thus, the stator employs three-phase single layer windings [10] with no iron teeth. This structure enables motors to close the field coils and the armature windings compared to the typical double-layer windings.

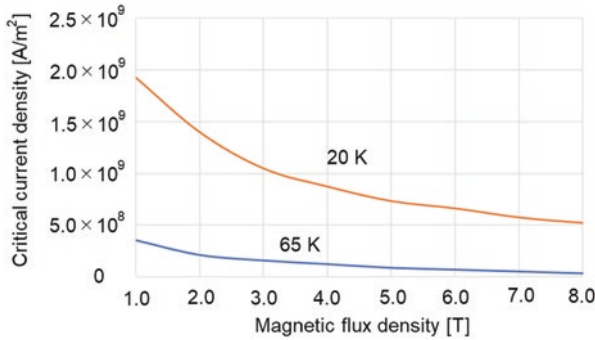


Fig. 3 Assumed critical current of the YBCO wire (4.0 mm × 0.1 mm rectangle) as a function of magnetic flux density based on a reference [9]

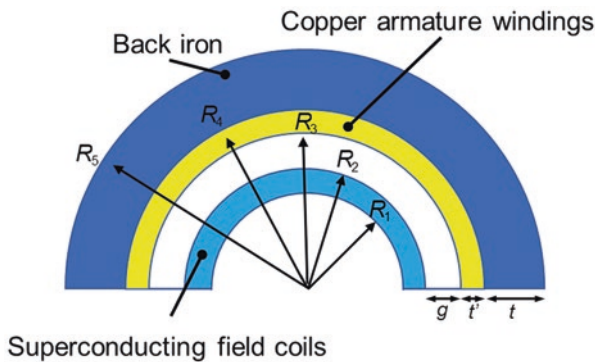


Fig. 4 Analysis model of a PSCM for EAPS

### 4 Output Power Density and Loss Estimate

Figure 4 shows the analytical model of the PSCM for electrified aircraft propulsion. The model is composed of field coils, armature windings, and back iron. The thickness of the components and mechanical gaps between the field coils and armature windings is  $t$  [m],  $t'$  [m], and  $g$  [m] as shown in Fig. 4. We set the  $g$  of PSCMs at 35 mm for vacuum and the cryostat wall space.

We conducted electromagnetic design based on several equations under full loaded and steady-state conditions. The PSCM's output power  $P_G$  [W] is given by

$$P_G = \frac{\pi^2}{\sqrt{2}} k_w B_m A_s D^2 I_{\text{eff}} \frac{N_{\text{rot}}}{60} \tag{1}$$

where  $k_w$  is the winding factor,  $B_m$  [T] is the magnetic loading (the amplitude of magnetic flux density from field current at the middle of armature windings),  $A_s$  [A/m] is the electric loading,  $D$  [m] is the average diameter of armature windings,

$l_{\text{eff}}$  [m] is the effective length of the motor, and  $N_{\text{rot}}$  [rpm] is the rotational speed. This is a fundamental equation, and we calculated the motor effective length  $l_{\text{eff}}$  [m] by setting individual variables based on Table 1 conditions shown in the previous chapter.

Each radius  $R_1 - R_5$  [m] is set as to satisfy the conditions used in Eq. (1). The magnetic flux density distribution generated by field current between the field coils and the back iron is calculated by following equation as a function of radial direction  $r$  [m], mechanical angle  $\theta$  [rad], and harmonic number  $n$  based on references [11, 12].

$$B(r, \theta, n) = \frac{4\mu_0 J_f}{\pi n(np+2)} \sin \frac{n\pi}{2} \sin \frac{n\pi}{6} \cos \frac{n\pi}{4} \cos(np\theta) (R_2^{np+2} - R_1^{np+2}) \left( \frac{r^{np-1}}{R_4^{2np}} + r^{-np-1} \right) \quad (2)$$

In this analysis, we assumed the magnetic loading  $B_m$  [T] to the amplitude of basic sinusoidal wave ( $n = 1$ ) at the middle of armature windings calculated by Eq. (2).

And we estimated the output power density of the PSCMs from these radius  $R_1 - R_5$  [m] and the effective length  $l_{\text{eff}}$  [m] by calculating the amount of materials in Fig. 1 and densities listed in Table 3. Then, we assumed the structures of the field coils and the armature windings as shown in Figs. 5 and 6, respectively. The average lengths of the field coils  $l_{\text{YBCO}}$  [m] and the armature windings  $l_{\text{Cu}}$  [m] are defined as follows:

$$l_{\text{YBCO}} = 2l_{\text{eff}} + R_2 (\theta_{f1} + \theta_{f2}) \quad (3)$$

$$l_{\text{Cu}} = \frac{2D\pi}{mp} + 2l_{\text{eff}} + 4\theta_a l_{\text{eff}} \quad (4)$$

**Table 3** Densities of the PSCM components

Description	Material	Density
Stator		
Back iron	Electromagnetic steel	7850 kg/m <sup>3</sup>
Armature windings	Copper wire	8960 kg/m <sup>3</sup>
Support structure	FRP	1900 kg/m <sup>3</sup>
Rotor		
Field coils	YBCO wire	8250 kg/m <sup>3</sup>
Shaft	SUS	7800 kg/m <sup>3</sup>
Torque tube	FRP	1900 kg/m <sup>3</sup>
Support structure	FRP	1900 kg/m <sup>3</sup>
Cryostat	SUS	7800 kg/m <sup>3</sup>

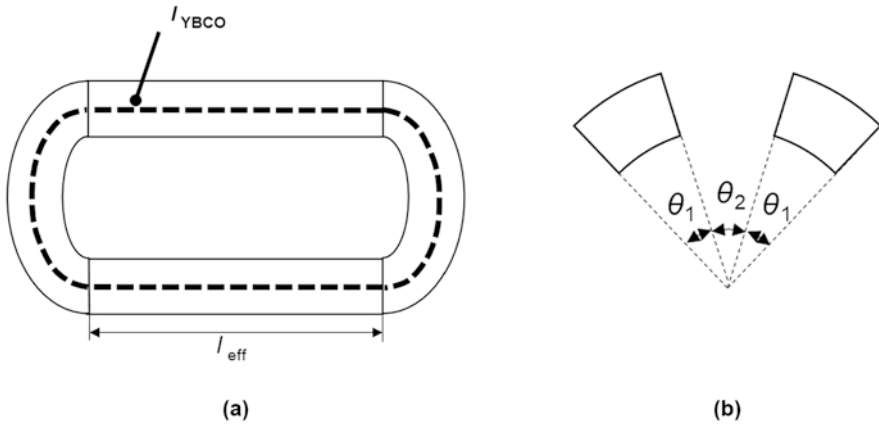


Fig. 5 Structure of the field coils. (a) is the top view and (b) is the cross section

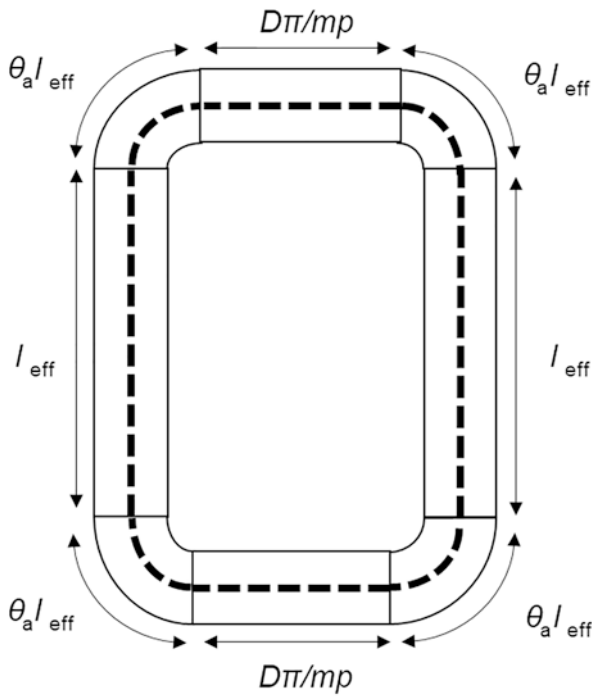


Fig. 6 Structure of the copper armature windings

where  $\theta_{\beta}$  [rad] is the angle of one field coil,  $\theta_{\beta}$  [rad] is the angle between the field coils,  $m$  is the number of phases ( $m = 3$ ),  $p$  is the number of pole pairs, and  $\theta_a$  is the factor at bending points.

The iron losses of the back iron and copper loss are considered in this study to estimate the efficiency of the PSCMs. The following equations represent hysteresis loss of the back iron  $W_{\text{iron,hys}}$  [W/m<sup>3</sup>] and eddy current loss of the back iron  $W_{\text{iron,eddy}}$  [W/m<sup>3</sup>]:

$$W_{\text{iron,hys}} = k_h \epsilon \frac{f}{100} B_{\text{iron}} \quad (5)$$

$$W_{\text{iron,eddy}} = k_e \sigma \left( \frac{f}{100} B_{\text{iron}} \right)^2 \quad (6)$$

where  $B_{\text{iron}}$  [T] is magnetic flux density at the back iron,  $k_h$  and  $k_e$  are rotation factors,  $\epsilon$  and  $\sigma$  are coefficients. The parameters used in this paper are shown in Table 4.  $B_{\text{iron}}$  [T] is set to 2.0 T which is the maximum saturated magnetic flux density of general iron. And copper loss  $W_{\text{Cu}}$  [W] is calculated by applying Ohm's law.

## 5 Analysis Results

We estimated the output power densities of the 5.5 MW PSCMs with different poles and operating temperature at different magnetic loadings based on Table 1. The diameters of motors were set as to maximize the output power density below 800 mm after selecting magnetic loadings. Finally, we found the magnetic loading that achieves the highest output power density. Figures 7 and 8 show the output power densities at each operating temperature as a function of magnetic loading. Some cases, in particular, at operating temperature of 65 K have high magnetic loading and were not able to be designed in order to satisfy the required motor diameter. This is because the high magnetic loading machine requires large amount of the field coils and the back iron. In addition, the high operating temperature of the field coils leads to the increase of the amount of field coils because of the  $J_c$ - $B$  characteristics of YBCO wires shown in Fig. 3. As shown in Figs. 7 and 8, the output power densities were improved by increasing the number of poles up to 12 because the amount of back iron was reduced. However, the output power densities of the

**Table 4** Parameters for equations of iron losses

Parameter	Value
Rotation factor $k_h$	2.0
Rotation factor $k_e$	1.8
Coefficient $\epsilon$	3.7
Coefficient $\sigma$	3.4



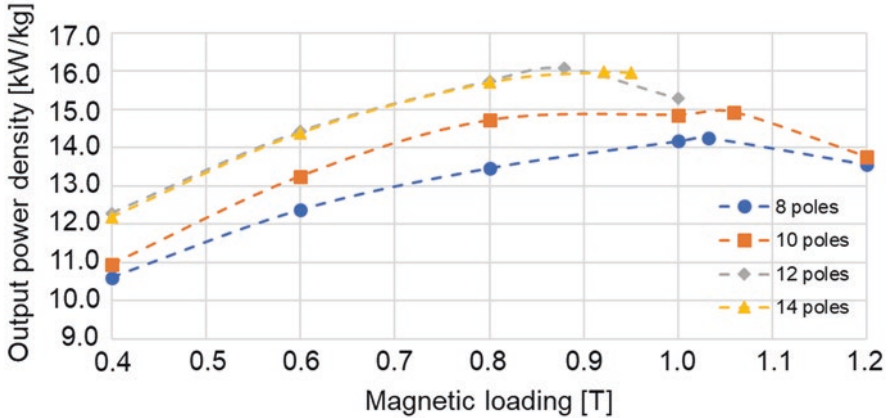


Fig. 7 Output power density of the 5.5 MW PSCMs at operating temperature of 20 K as a function of magnetic loading with different poles

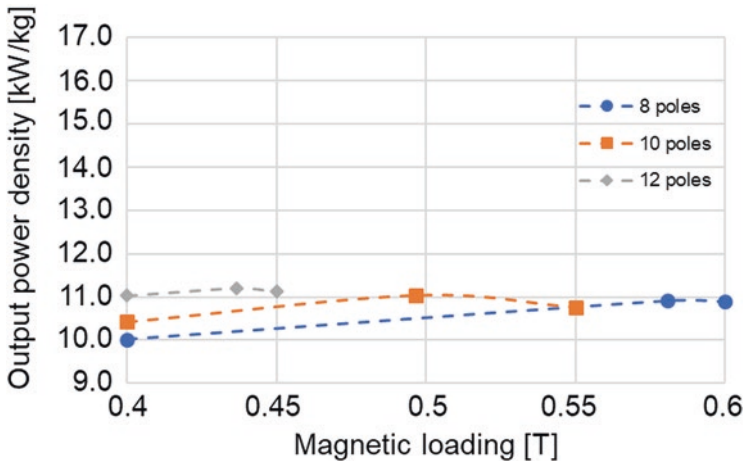


Fig. 8 Output power density of the 5.5 MW PSCMs at operating temperature of 65 K as a function of magnetic loading with different poles

14-pole PSCMs were decreased compared to the 12-pole PSCMs because the amount of the YBCO wires was increased. The output power density of 16.1 kW/kg with 12 poles at 0.88 T at 20 K and of 11.2 kW/kg with 12 poles at 0.44 T at 65 K was available. The output power density of the PSCM at 20 K attains the 16 kW/kg. However, the output power density at 65 K did not reach the required value, although, the value is much higher than that of conventional electric motors. Tables 5 and 6 show the weights and losses of PSCM components, respectively. The weight margin of 25% for the stator and the rotor is considered. The motor efficiency is calculated from the copper loss and the iron losses at the back iron. The AC loss at

**Table 5** Summary of the PSCM component weights

Description	Design at 20 K	Design at 65 K
<b>Stator</b>		
Back iron	88.3 kg	86.9 kg
Armature windings	44.6 kg	75.4 kg
Support structure	4.3 kg	7.0 kg
25% margin	34.3 kg	42.3 kg
<b>Rotor</b>		
Field coils	9.0 kg	28.9 kg
Shaft	4.6 kg	6.1 kg
Torque tube	3.2 kg	4.2 kg
Support structure	10.3 kg	16.3 kg
Exciter	14.0 kg	14.0 kg
25% margin	41.0 kg	69.6 kg
Cryostat	88.7 kg	140.2 kg
Total weight	342.2 kg	491.1 kg
Output power density	16.1 kW/kg	11.2 kW/kg

**Table 6** PSCM loss components

Parameter	Design at 20 K	Design at 65 K
Copper loss	52.4 kW	88.6 kW
Hysteresis loss at back iron	5.3 kW	5.2 kW
Eddy current loss at back iron	21.9 kW	21.6 kW
Efficiency	98.6%	97.9%

the field coils was not considered because the field coils only experience DC field under steady-state condition.

## 6 Electromagnetic Design with Finite Element Method Analysis

Two-dimensional finite element method (FEM) analysis with the electromagnetic analysis software, JMAG-Designer<sup>®</sup> [13], was carried out for electromagnetic design of the 5.5 MW PSCMs based on the designs that represent maximum output power density at operating temperature of 20 K and 65 K shown in the Chap. 5 to testify the designed PSCMs' output calculated output power. Figure 9 shows the one pole pitch of analysis model of a 12-pole PSCM. The analytical model is composed of the YBCO field coils, the copper armature windings, and the back iron. For simplicity, any other non-magnetic components such as cryostat wall are not taken into account in the analysis model.

Tables 7 and 8 show the comparison of the analytical and the FEM results of 5.5 MW PSCMs, whose operating temperatures of the field coils are 20 K and 65 K,

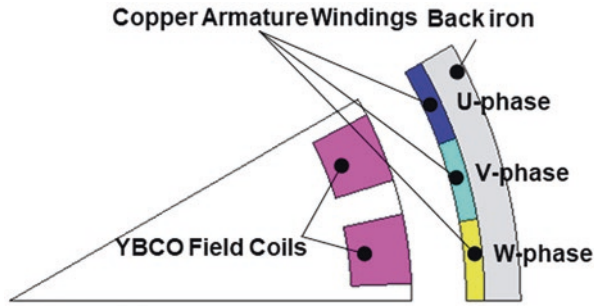


**Fig. 9** One pole pitch of the analysis model of a 12-pole PSCM

**Table 7** Comparison of the analytical and FEM results of 5.5 MW PSCM at operating temperature of 20 K

Parameter	Theoretical	FEM	Error
Torque	10,504 nm	10,521 nm	0.2%
Magnetic loading	0.88 T	0.92 T	4.7%
Max. of magnetic flux density at field coils	2.50 T	2.53 T	1.2%
Iron losses at back iron	27.2 kW	42.8 kW	36.4%
Output power	5.50 MW	5.51 MW	0.2%
Output power density	16.1 kW/kg	16.1 kW/kg	0.2%

respectively. Four parameters, motor torque, magnetic loading (amplitude of magnetic flux density at the middle of the armature windings), maximum of magnetic flux density at the field coils, and the iron losses at the back iron, were compared in this analysis. The output power densities of the FEM analysis were calculated from the motor torques shown in Tables 7 and 8 and the motor weight obtained by equations in the previous chapter. The errors of the motor torque, the magnetic loading, and the maximal magnetic flux density at the field coils are within the range of 7%. On the other hand, iron losses at the back iron differ over 30% between the theoretical and FEM results because Eqs. (5) and (6) calculate the iron losses at the back iron. However, the iron losses are relatively small compared to copper losses shown in Table 6. Also, the differences of the iron losses are below 0.3% compared to the total output power. Finally, the output power densities of the PSCMs are 16.1 kW/kg and 12.0 kW/kg at the operating temperature of 20 K and 65 K, respectively.

## 7 Conclusion

Electromagnetic design of the 5.5 MW partially superconducting motors was carried out at different operating temperatures, 20 K and 65 K. The estimated output power density results are as follows: 16.1 kW/kg at 20 K and 12.0 kW/kg at 65 K. The output power density at 20 K attains the required value. Therefore,

**Table 8** Comparison of the analytical and FEM results of 5.5 MW PSCM at operating temperature of 65 K

Parameter	Theoretical	FEM	Error
Torque	10,504 nm	11,274 nm	6.8%
Magnetic loading	0.44 T	0.46 T	4.8%
Maximal of magnetic flux density at field coils	1.12 T	1.08 T	3.7%
Iron losses at back iron	26.8 kW	42.4 kW	36.9%
Output power	5.50 MW	5.90 MW	6.8%
Output power density	11.2 kW/kg	12.0 kW/kg	6.8%

partially superconducting motors operated at 20 K could be a potential candidate for the future electrified aircraft propulsion system. On the other hand, the estimated output power density at 65 K does not reach the required value, 16 kW/kg. However, it is much higher than that of the conventional electric motors.

## References

1. H. Kim, J. Felder, M. Tong, J. Berton, W. Haller, *Turboelectric distributed propulsion benefits on the N3X vehicle*. *Aircr. Eng. Aerosp. Technol. Int. J.* **86**(6), 558–561 (2014). Can be downloaded at: <https://doi.org/10.1108/AEAT-04-2014-0037>
2. <https://www.airbus.com/innovation/The-future-is-electric.html>
3. <https://www.siemens.com/press/pool/de/events/2016/corporate/2016-12-innovation/inno2016-aerobaticairplane-e.pdf>
4. B. Łukasik, *Turboelectric distributed propulsion system as a future re-placement for turbofan engines*, in Proceedings of the ASME Turbo Expo 2017: Turbomachinery technical conference and exposition (Charlotte, America, 26–30 June 2017). ISBN:978-0-7918-5077-0. Can be downloaded at: <http://proceedings.asmedigitalcollection.asme.org/proceeding.aspx?articleid=2649486>
5. H. Ohsaki, Technology trends of superconducting rotating machines. *J. Cryog. Supercond. Japan* **47**(6), 354–361 (2012). ISSN:0389-2441
6. C. Jones, P. Norman, S. Galloway, M. Armstrong, A. Bollman, *Comparison of candidate architectures for future distributed propulsion aircraft*. *J. IEEE Trans. Appl. Supercond.* **26**(6), 1–9 (2016). Can be downloaded at: <https://ieeexplore.ieee.org/document/7407568>
7. M. Zhang, F. Eastman, W. Yuan, *Design and modeling of 2G HTS armature winding for electric aircraft propulsion applications*. *J. IEEE Trans. Appl. Supercond.* **26**(3), 1–5 (2016). Can be downloaded at: <https://ieeexplore.ieee.org/document/7428847>
8. <http://787updates.newairplane.com/787-Electrical-Systems/787-Electrical-System>
9. <http://www.superpower-inc.com/system/files/1MOr2A-03++Superpower-Inc+ASC-2016+Final.pdf>
10. S. Kalsi, K. Hamilton, R. Badcock, *Superconducting rotating machines for aerospace applications*, Meeting paper of the AIAA Propulsion and Energy Forum (Ohio, America, 9–11 July 2018). Can be downloaded at: <https://doi.org/10.2514/6.2018-4796>
11. S. Kalsi, *Applications of High Temperature Superconductors to Electric Power Equipment* (Wiley, 2011). ISBN:978-0-470-16768-7
12. Shintani T. Nitta T. and Okada T. *Explicit relations between machine constants and structure-parameters of superconducting generators*. *J. IEEE Trans. Power Energy*, 106, 12, pp. 1075–1082, 1986. Can be downloaded at: <https://doi.org/10.1541/ieejpes1972.106.1075>
13. <https://www.jmag-international.com/jp/products/jmag-designer/>